Solar Energy Materials and Solar Cells 195 (2019) 174–181

Contents lists available at ScienceDirect

Solar Energy Materials and Solar Cells

journal homepage: www.elsevier.com/locate/solmat

Kinetics and dynamics of the regeneration of boron-oxygen defects in compensated n-type silicon

Chang Sun[a,*], Daniel Chen[b], Fiacre Rougieux[b], Rabin Basnet[a], Brett Hallam[b], Daniel Macdonald[a]

[a] Research School of Engineering, The Australian National University, Canberra, ACT, 2601, Australia
[b] School of Photovoltaic and Renewable Energy Engineering, University of New South Wales, Kensington, NSW, 2052, Australia

ARTICLE INFO

Keywords:
Light-induced degradation
Boron
Oxygen
Regeneration
Compensated
n-type silicon

ABSTRACT

The effects of doping level, illumination intensity and temperature on the regeneration kinetics and dynamics of BO defects in compensated n-Si have been investigated. The regeneration rate, corrected with interstitial oxygen concentration and average injection level, is almost constant in n-type samples with different doping levels under the same regeneration condition. It is proportional to the average injection level during regeneration when the doping level and temperature are fixed. In comparison with previous studies using n-type silicon, the regeneration completeness is significantly improved, especially in samples with net doping levels higher than $1 \times 10^{16}\,cm^{-3}$, due to the higher regeneration temperature and more stable surface passivation films. The remaining incompleteness is mostly dominated by the occupation of the annealed state (as opposed to the activated state). For rapid and complete regeneration, the optimal condition is applying high illumination intensities at around 200°C.

1. Introduction

The Boron-Oxygen-related (BO) defect, which causes the degradation of carrier lifetime of B-doped Czochralski (Cz) silicon materials under carrier injection, has been intensively studied in the past decades [1–8]. It has been shown that this defect can be permanently deactivated (regenerated) by annealing at elevated temperatures with carrier injection from illumination or an applied bias [6–11]. In p-type silicon (p-Si), a complete elimination of the defects can be achieved within seconds by applying high illumination intensities [12–14].

Conventional n-type Cz material grown using the Siemens process is free from BO related degradation due to the absence of boron dopants. However, for upgraded metallurgical grade (UMG) n-type silicon purified using alternative pathways, the compensated nature of the material with the presence of both boron and phosphorus dopants in the silicon means that it is also susceptible to BO degradation [6,15–20]. The defect in n-type silicon (n-Si) is also of both research and industrial interest. Comparisons of the same defect properties in both n- and p-Si have helped to improve the fundamental understanding of the defect significantly [16,17,21–24]. The potential of low-cost n-type upgraded metallurgical-grade (UMG) Cz silicon materials for high-efficiency solar cells has been demonstrated in multiple studies, with efficiencies above 20% reported [25–28]. However, the susceptibility to BO defects remains a disadvantage of such materials [26,29].

Several previous studies have attempted the regeneration of BO defects in n-Si. However, they have reported less consistent results in comparison to that for studies investigating p-Si. In Ref. [4], the recovered lifetime after illuminated annealing was observed to be unstable during subsequent light soaking. It was discussed in Ref. [30] that the unstable lifetime was due to the fact that a significant fraction of the defects were annealed instead of regenerated during the illuminated annealing. Complete regeneration of BO defects in an n-type sample with a doping level $n_0 = 1.5 \times 10^{16}\,cm^{-3}$ was reported in Ref. [31], however, the long-time stability of the regeneration was not confirmed. In Ref. [30], n-type samples with various doping levels were regenerated and the long-time stability test was conducted. The completeness of regeneration was 80–90% in samples with net doping levels in the range of 10^{15}–$10^{16}\,cm^{-3}$. However, this was reduced to 50% and below in the two samples with $n_0 > 1 \times 10^{16}\,cm^{-3}$. Recently we have demonstrated complete regeneration in n-type UMG Cz silicon heterojunction solar cells with $n_0 = 1 \times 10^{15}\,cm^{-3}$ and $7 \times 10^{15}\,cm^{-3}$ [32]. A more detailed study on how the regeneration is affected by the processing parameters and sample doping levels will be valuable.

In this study, we examine the effects of three parameters 1) doping level, 2) illumination intensity I, and 3) temperature T, on the regeneration of BO defects in compensated n-Si, to determine if the completeness can be further improved from those values in the literature. We measure and analyse both the regeneration kinetics and

* Corresponding author.
E-mail address: chang.sun@anu.edu.au (C. Sun).

https://doi.org/10.1016/j.solmat.2019.03.016
Received 31 October 2018; Received in revised form 12 February 2019; Accepted 6 March 2019
Available online 15 March 2019

Table 1
Doping levels and [O_i] of the compensated Cz samples used in this work.

g	Modelled [B] ($\times 10^{16}$ cm^{-3})	Modelled [P] ($\times 10^{16}$ cm^{-3})	Measured or interpolated [P]-[B] ($\times 10^{15}$ cm^{-3})	[O_i] ($\times 10^{17}$ cm^{-3})
0.05	4.71	4.22	−2.3 (SIMS)	9.1
0.24	4.98	4.83	3.5 (interpolated)	8.1
0.31	5.09	5.08	5.6 (ECV)	8.0
0.36	5.19	5.32	6.2 (interpolated)	8.0
0.41	5.30	5.58	6.8 (ECV)	7.8
0.52	5.58	6.31	10 (ECV)	7.5
0.67	6.15	7.94	17.5 (interpolated)	6.7
0.74	6.53	9.13	20 (ECV)	6.5
0.83	7.24	11.65	29 (ECV)	6.1

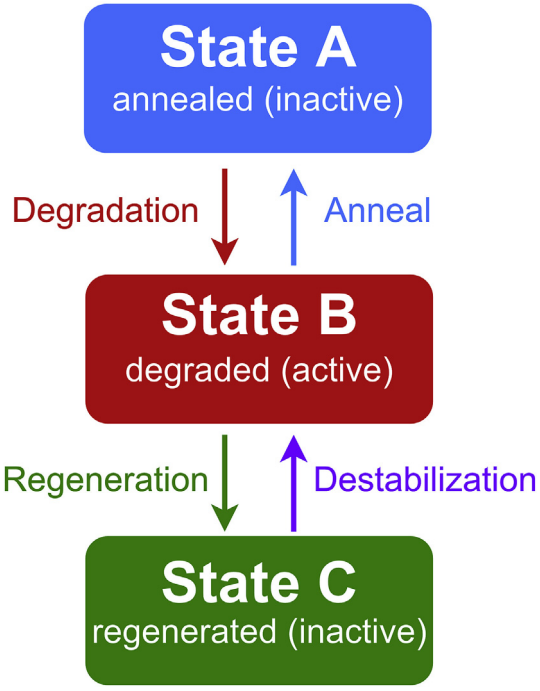

Fig. 1. Three-state model of the BO defect based on Refs. [10,14].

dynamics (the defect state occupation under final steady-state conditions) to gain deeper understanding of the state transitions of the defect during the regeneration in compensated n-Si.

2. Experimental methods

The samples were from different solidified fractions, g, of a B- and P-doped compensated Cz ingot grown with electronic-grade feedstock. The concentrations of B and P ([B] and [P]) in the starting melt of the ingot were 6.2×10^{16} cm^{-3} and $(10 \pm 1) \times 10^{16}$ cm^{-3}, respectively. The [B] and [P] in the samples were calculated by applying Scheil's law, and are shown in Table 1. The segregation coefficients of B and P were taken as 0.75 and 0.41, respectively, as determined in Ref. [18]. The [B] and [P] in some of the samples were measured by secondary ion mass spectrometry (SIMS), and the net doping was measured by electrochemical capacitance voltage (ECV) measurements [18], as also shown in Table 1. The net doping levels of other samples were interpolated based on both SIMS and ECV results. Note that as confirmed by SIMS and ECV measurements, only the sample from $g = 0.05$ is p-type. All other samples are n-type. A more detailed analysis of the doping levels of the samples can be found in Ref. [18]. The interstitial oxygen concentrations ([O_i]) in the samples shown in Table 1 were determined by Fourier Transform Infrared (FT-IR) spectrophotometry [16].

The samples were saw damage etched with tetramethylammonium hydroxide (TMAH) solution, and then went through a phosphorus gettering process at 785 °C for 0.5 h, to remove fast diffusing metallic impurities. After removing the diffused layers, Plasma-Enhanced Chemical Vapour Deposited (PECVD) hydrogenated silicon nitride (SiN_x:H) films were deposited on both sides of the samples as surface passivation in a Roth and Rau AK400 chamber. The temperature during the deposition was about 250 °C, measured on the samples. The deposition time was 3 min. The thickness of the SiN_x:H film on each side of the sample was about 80 nm. The refractive index of the film is 1.99 for the wavelength of 632.8 nm. To accelerate the regeneration process [33], an intentional firing step at 600 °C for 5 s, with a 30 °C/s ramp up rate, and average ramp down rate of approximately 14 °C/s, was performed on all the coated samples in a Rapid Thermal Processor (RTP). The temperature was measured on the sample. The processing parameters of the firing step were previously optimised for this SiN_x film, based on the hydrogenation effects of grain boundaries in multicrystalline wafers [34]. Subsequently, the SiN_x:H films were removed in dilute hydrofluoric (HF) acid solution. Then, the samples were re-cleaned and re-passivated with the same SiN_x:H films for subsequent measurements. Several non-compensated n-type Cz wafers with $[P] = 5 \times 10^{15}$ cm^{-3} were also included in the study as control wafers. They went through the same firing step with SiN_x:H films, and were also re-passivated with the same fresh SiN_x:H films.

The lifetime measurements were conducted *ex-situ* with a Sinton Instruments WCT-120 Quasi-Steady-State Photo-Conductance (QSSPC) lifetime tester. The mobility model in Ref. [35] was used to estimate the carrier mobility in compensated silicon. The lifetime values in the following discussion are reported at an injection level of $\Delta n = 0.3 n_0$ (or $0.3 p_0$ for the p-type sample) [20,30].

The three-state model of the BO defect is shown in Fig. 1, based on Ref. [10,14]. We describe the following processing and measurements based on this model.

First, the background lifetime $\tau_{background}$ was measured when all the BO defects in the inactive State A, achieved by a dark annealing step at 250 °C for 40 min [20]. How the dark annealing affects the regeneration kinetics and dynamics [12] needs to be further assessed in the future work. Then the samples were subjected to light soaking under 3–4 suns, to reach State B. The illumination was provided by a halogen lamp, and the intensity was measured by a reference cell [36]. The temperature of the samples was controlled below 45 °C. We observed that it took 1–2 days for the lifetime of the samples from lower solidified fractions to saturate, and 7–8 days for those from higher solidified fractions. To ensure that all the samples went through the same illumination and thermal history, we fixed the time length of the light soaking step as 8 days for all the samples. No recovery of lifetime was observed on any samples at this stage. The lifetime after light soaking was measured, and denoted as $\tau_{degraded}$.

We then measured three groups of regeneration data:

2.1. Group 1: the doping-dependent group

The first group contains one sample at each g value in Table 1. The temperature of the sample during the regeneration was controlled at

180 ± 5 °C on a hotplate. The illumination intensity was 10.5 ± 1 suns, measured by a reference cell and provided by a broadband halogen lamp. The uncertainties in the temperature are introduced by the non-uniform heating by the halogen lamp.

2.2. Group 2: the I-dependent group

Group 2 contains 4 samples from $g = 0.74$ of the ingot. They were regenerated at 180 ± 5 °C, under 1 sun, 2 suns, 4.5 suns, and 93 suns, respectively. The three lower illumination intensities were provided by the halogen lamp. The 93-sun illumination was provided by a 938 nm laser, with 57 kW/m^2 illumination intensity [14]. The photon flux was equivalent to 93 suns, based on the reference spectrum ASTM G173 [36].

2.3. Group 3: the temperature (T)-dependent group

Group 3 contains another 5 samples from $g = 0.74$ of the ingot. They were regenerated under 10.5 ± 1 suns, at 155 ± 5 °C, 195 ± 5 °C, 228 ± 6 °C, 244 ± 6 °C, 264 ± 5 °C, respectively. The temperatures were measured on the samples under illumination. The uncertainties are mainly due to the non-uniform heating by the lamp. In the results and discussion, the sample from $g = 0.74$ from Group 1 is also included in this group and Group 2.

For all the samples, we measured the regeneration kinetics until the lifetime saturated. The saturated lifetime is denoted as $\tau_{regenerated}$. A stability test was performed after regeneration, under 3–4 suns at < 45 °C for 8 days. The lifetime after the stability test τ_{stable} was measured.

For each sample from $g = 0.74$ (from all 3 groups), the same illuminated annealing (same I, T and time) and measurements were performed on a non-compensated Cz control sample to monitor the change in the background lifetime.

3. Data analysis

3.1. Kinetics

The relative defect concentration at time t is

$$N_t^*(t) = \frac{1}{\tau_{eff}(t)} - \frac{1}{\tau_{background}}, \quad (1)$$

with the lifetime extracted at $\Delta n = 0.3n_0$ (or $0.3p_0$ for the p-type sample) The relative defect concentrations during regeneration were then fitted with

$$N_t^*(t) = C_1 + C_2 exp(-R_{regen}t), \quad (2)$$

where C_i is a constant and R_{regen} is the regeneration rate [4].

3.2. Dynamics

The concentrations of the three states after regeneration can be calculated with the lifetime measured at several key time points. During the stability test, States B and C do not change, while State A will turn to State B. So the concentration of State A after regeneration can be calculated as

$$N_A^* = \frac{1}{\tau_{stable}} - \frac{1}{\tau_{regenerated}}. \quad (3)$$

After the regeneration, only State B is recombination-active, thus it can be obtained as

$$N_B^* = \frac{1}{\tau_{regenerated}} - \frac{1}{\tau_{background}}. \quad (4)$$

There are fewer defects that are activated during the stability test, than during the initial light soaking step, due to the regenerated fraction. Therefore

$$N_C^* = \frac{1}{\tau_{degraded}} - \frac{1}{\tau_{stable}}. \quad (5)$$

The fraction occupied by State i ($i = A, B, C$) is

$$f(i) = \frac{N_i^*}{N_A^* + N_B^* + N_C^*}. \quad (6)$$

The analogous N_A^* and N_B^* in the control samples can also be calculated. N_A^* and N_B^* in the control samples indicate the change in the background lifetime during the stability test, and during the light soaking step and regeneration, respectively. The change in the background lifetime of the control wafers is mainly due to the instable surface passivation during the processes [37]. We assume that the background lifetimes of both the experimental sample and the corresponding control sample have been through the same changes during the processes. We note that the validness of this assumption could be complicated by the dopant and carrier density dependent degradation of background lifetime in different wafers [37]. In order to evaluate this effect in the experimental samples, the analogous fractions $f_{control}$(A) and $f_{control}$(B) were calculated using N_A^* and N_B^* in the control samples, and the average value of $\sum N_i^*$ in the samples from $g = 0.74$.

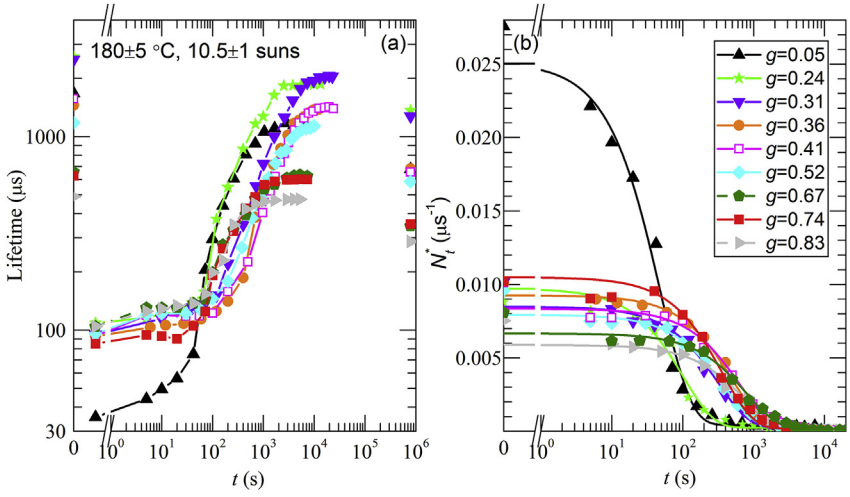

Fig. 2. (a) Evolution of lifetime during regeneration at 180 ± 5 °C under 10.5 ± 1 suns, measured on samples from Group 1. The solid lines are guides to the eye. (b) Evolution of the relative defect concentration during regeneration. The solid lines are exponential fits. In (a), $\tau_{background}$ is shown at 0 s, $\tau_{degraded}$ is shown before the axis break, and τ_{stable} is shown at about 10^6 s.

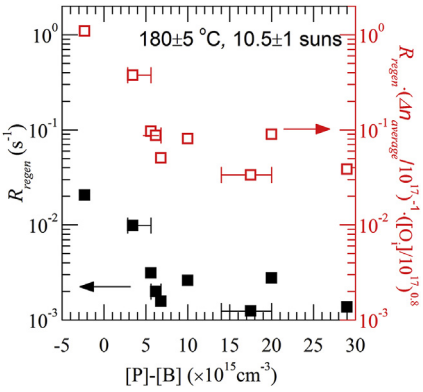

Fig. 3. Defect regeneration rates at 180 ± 5 °C under 10.5 ± 1 suns as a function of [P]-[B] (solid squares), and after correction for oxygen concentration and injection level (open squares).

4. Results and discussion

4.1. Group 1: the doping-dependent group

Fig. 2 shows the regeneration kinetics of Group 1, and the fitting of the extracted relative defect concentration. The fitted regeneration rates are shown in Fig. 3, as a function of net doping. To increase the comparability of different samples, we corrected R_{regen} assuming that $R_{regen} \propto [O_i]^{-0.8}$ [38], and that $R_{regen} \propto \Delta n_{average}$ [39], as shown in the open squares in Fig. 3. The linear dependence of R_{regen} on $\Delta n_{average}$ will be further discussed in 4.2. As the injection level increases during the regeneration under fixed illumination intensity, the average value $\Delta n_{average}$ of the lowest and highest injection levels was used [38,39]. The lowest and highest injection levels were estimated using $\tau_{degraded}$ and $\tau_{regenerated}$ (measured at room temperature) respectively. As shown, the corrected regeneration rates are quite similar in the n-type samples with different doping levels. This is different to p-Si, where the regeneration rate was found to decrease with increasing total dopant concentration [4,38]. This finding agrees with Ref. [4], which reported an approximately constant value of R_{regen} in n-type samples with different doping levels. However, in that work the regeneration was found to be unstable/incomplete.

The occupation of the three states after regeneration is shown in Fig. 4, as a function of the net doping. The completeness of the regeneration is f(C). It is 97% in the p-type sample, 91%–96% in the n-type samples with $n_0 \leq 1 \times 10^{16}\,cm^{-3}$, and 80%–90% in those with $n_0 > 1 \times 10^{16}\,cm^{-3}$. The regeneration is more complete in comparison with Ref. [30], especially in the samples with $n_0 > 1 \times 10^{16}\,cm^{-3}$. The higher completeness in this work could be attributed to the higher regeneration temperature applied, and more stable silicon nitride films [30], which will be further discussed in the following sections. Fig. 4 also shows that the incompleteness is dominated by the occupation of State A, which increases with increasing [P]-[B]. However, because the data in this group are not corrected with control samples, other effects such as the degradation of surface passivation could be included into the fractions of the states [37].

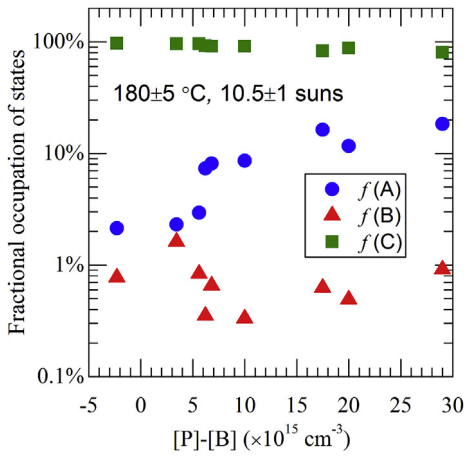

Fig. 4. The fractions occupied by the three states after regeneration in Group 1, as a function of [P]-[B]. States A and C were differentiated by the stability test after regeneration.

4.2. The kinetics in Group 2

Fig. 5 shows the second group of the regeneration kinetics, and the fitting of relative defect concentrations. The five samples have similar lifetimes after dark annealing, and after light soaking. The evolution of the lifetime showed two-stage kinetics in all of the samples. In the first stage, an initial "quasi steady state" was reached, which is dominated by the transitions between State A and State B. This happened because the samples were degraded at < 45 °C under 3–4 suns, but then brought under the regeneration conditions at 180 °C under 1–93 suns. The lifetime increased under 1–10 suns due to the deactivation (B to A) of some BO defects caused by the elevated temperature. We can see that a higher illumination intensity favours State B, due to the quadratic dependence of the activation rate (k_{AB}) on the injection level in n-Si [17,20]. The second stage is dominated by the regeneration (B to C). Note that in theory [40], the possible state transitions (A↔B and B↔C) occur simultaneously during the regeneration. The two stages could be observed mainly because different transitions are dominant over different time scales, due to the difference in the reaction rates (k_{AB}, k_{BA}; k_{BC}, k_{CB}).

The fitted regeneration rates are shown in Fig. 6, as a function of the illumination intensity and injection level. For the 93-sun illumination intensity, the injection level during the regeneration was significantly higher than the injection range where the lifetime was measured. The lower limit of the injection level was then simply taken as the highest measured injection level in $\tau_{degraded}$. The higher limit was calculated using the injection-dependent Auger recombination lifetime [41]. We then fitted the injection-dependent regeneration rate to a power law equation $R_{regen} = C_3 \Delta n^{\gamma}$. The fitted power γ is in the range of 1.1–2.3, with an optimal value of 1.2. This suggests that R_{regen} is proportional to Δn in n-Si. The same dependence was observed in p-Si in Ref. [39].

4.3. The kinetics in Group 3

Fig. 7 shows the regeneration kinetics of Group 3, and the fitting of relative defect concentrations. Similar to Group 2, two-stage regeneration kinetics were observed on all the samples. In the first stage, a higher temperature favours State A over State B, indicating that k_{BA} has a stronger dependence on the temperature than k_{AB} under fixed illumination intensity [40,42]. The fitted regeneration rates are shown in Fig. 8. As the completeness is significantly reduced at those high temperatures (which will be discussed in 4.5), large uncertainties are expected in the fitted regeneration rates in this group. It is also difficult to estimate the uncertainties as both the transitions to State A and to State C result in lifetime increase during the regeneration, yet they cannot be distinguished in the kinetics analysis [4,30]. Fitting the four lower-temperature data points with the Arrhenius equation gives an activation energy of 1.2 eV. The uncertainties in the fitted regeneration rates introduced by the uncertainties in the regeneration temperature (due to the non-uniform heating by the lamp) were estimated using this activation energy, and are shown in the error bars in the vertical direction in Fig. 8. It is not easy to do the same estimation for the data in Groups 1–2 as the activation energy was found to depend on the illumination intensity and may also on the doing level and compensation level [38].

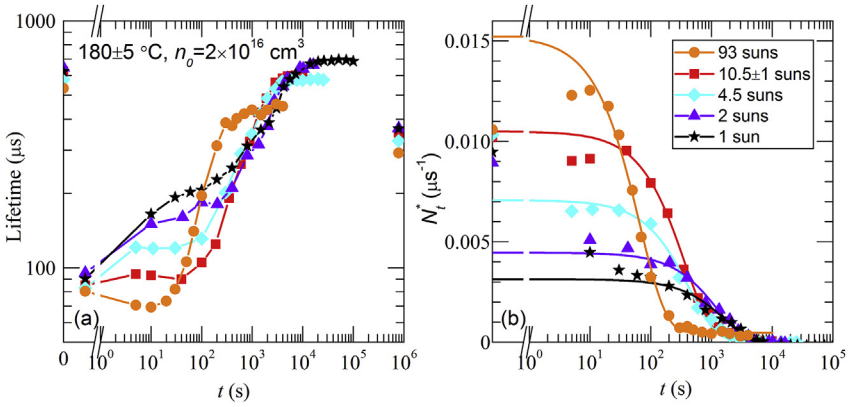

Fig. 5. (a) Evolution of lifetime during regeneration at 180 ± 5 °C under different illumination intensities. The solid lines are guides to the eye. (b) Evolution of the relative defect concentration during regeneration. The solid lines are exponential fits. In (a), $\tau_{background}$ is shown at 0 s, $\tau_{degraded}$ is shown before the axis break, and τ_{stable} is shown at about 10^6 s.

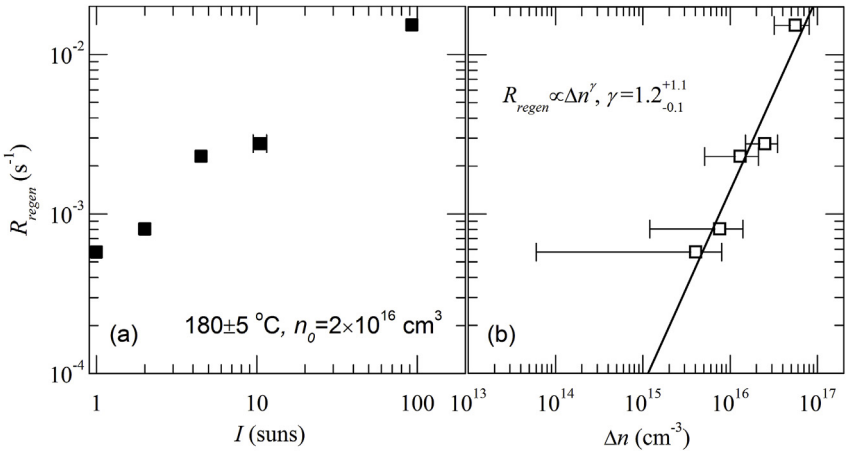

Fig. 6. The regeneration rate as a function of (a) illumination intensity, and (b) injection level.

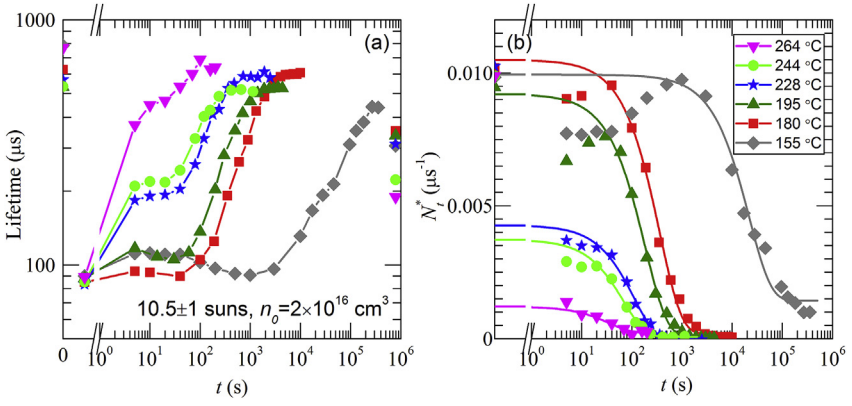

Fig. 7. (a) Evolution of lifetime during regeneration under 10.5 ± 1 suns at 155–264 °C. The solid lines are guides to the eye. (b) Evolution of the relative defect concentration during regeneration. The solid lines are exponential fits. In (a), $\tau_{background}$ is shown at 0 s, $\tau_{degraded}$ is shown before the axis break, and τ_{stable} is shown at about 10^6 s.

4.4. The control samples

Fig. 9 shows the regeneration kinetics measured on the control samples. The change of the effective lifetime is mainly due to the degradation and activation of the SiN_x:H films during illumination or annealing [37]. The firing step at 600 °C should not have created significant defects that are responsible for the light- and elevated temperature-induced degradation (LeTID) in these control samples [43]. The change in the background lifetime should not have significant effects on the defect kinetics analysis because: 1) the lifetime of the experimental samples varies in the 70–800 μs range, whilst the lifetime of the control samples varies in the 800–1800 μs range. Therefore the change in the background lifetime does not significantly affect the changes in the extracted N_t^*. 2) N_t^* could be affected when it becomes lower near the end of the regeneration. However, the lower-concentration data points are less important in fitting R_{regen}, because the sum of squared *absolute* deviations is minimized in the fitting.

However, the changes in the background lifetime *do* affect the dynamics analysis, mainly because several lifetimes ($\tau_{background}$, $\tau_{regenerated}$, and τ_{stable}) used in the dynamics analysis were measured when the sample contained the lowest active defect concentrations.

4.5. The dynamics in Groups 2 and 3

In Fig.s 10 and 11, we plot the fractional state occupations in Groups 2 and 3, together with $f_{control}$(A) and $f_{control}$(B). The three states are discussed as follows:

State A: As f(A) is always higher than the corresponding $f_{control}$(A),

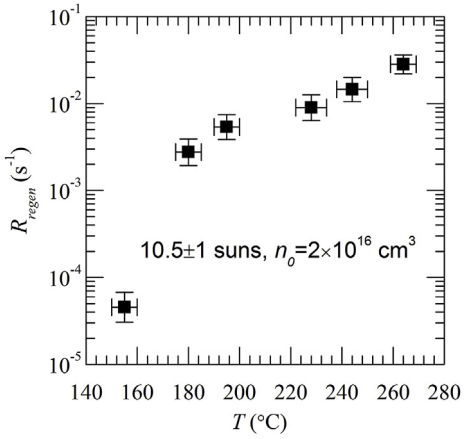

Fig. 8. The regeneration rate as a function of temperature.

the fractional occupation of State A can be corrected as f(A)-$f_{control}$(A), to get rid of the effects of background lifetime change. We can see that the incompleteness is dominated by the occupation of State A in most samples. It decreases with increasing I or decreasing T. This agrees with the theoretical model [14,40]: the illumination increases both k_{AB} and k_{BC}, thus decreasing State A; the temperature increases k_{BA} more than k_{AB}, and also increases k_{CB} more than k_{BC}, thus increasing State A. However, we note that the corrected fraction of State A only decreases 2% when the illumination increases from 1 sun to 93 suns (Fig. 10(a)). It could lie within the measurement error.

State B: f(B) is always very similar to $f_{control}$(B) as shown in the Fig.s, meaning that an unambiguous occupation by State B after regeneration cannot be concluded. The only exception is the sample regenerated at 150 °C: f(B) is much higher than $f_{control}$(B). A similar scenario was observed in Ref. [30]: during regeneration under 1 sun at 110 °C, the lifetime saturates at a value where N_t^* is well above 0. The reason could be: 1) a longer regeneration time is required for a more complete reaction; or 2) the background lifetime starts to degrade (as shown in Fig. 10), which compensates or even overcomes the bulk lifetime increase due to further regeneration of BO defects. Those reasons could potentially explain the lower completeness of regeneration observed in Ref. [30]: 1) the regeneration was conducted at a low temperature 110 °C, which significantly slows down the kinetics and prolongs the regeneration time; 2) The SiN_x:H films are less stable in Ref. [30], as significant degradation of the background lifetime was observed under 1 sun at 145 °C in less than 6 h [30].

State C: This is the regenerated BO defect state, representing the completeness of regeneration. As the background lifetime degradation is also included in the incompleteness (States A and B), the actual completeness should be higher than f(C) shown in the figures. The

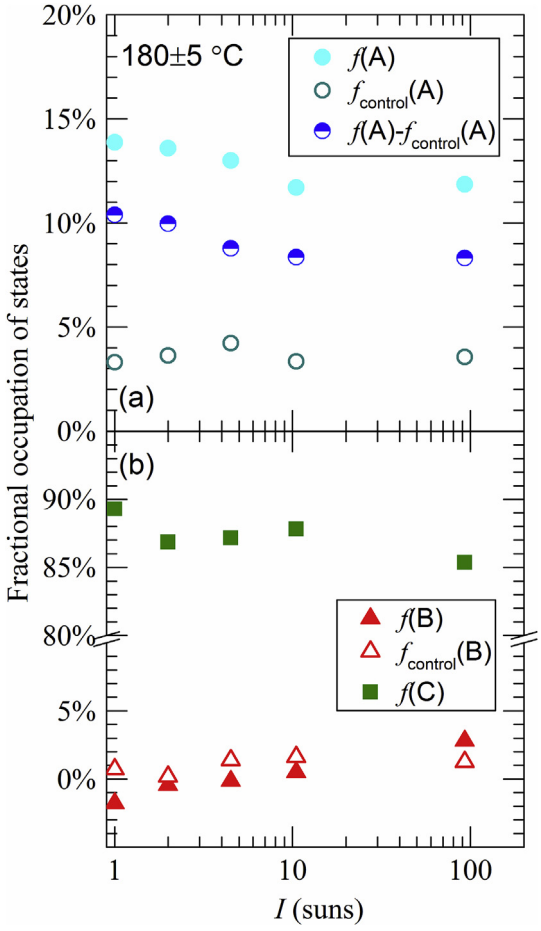

Fig. 10. The fractions occupied by the three states after regeneration, as a function of illumination intensity.

completeness is very similar in samples in Group 2, in the range of 85–90%. In Group 3, similar completeness is achieved at 180–230 °C, but is reduced at lower or higher temperatures, due to the occupation of State B or State A, as discussed above.

The presence of the control samples has made the conclusions more reliable. Without them, f(A) and f(B) are likely to be overestimated and f(C) underestimated.

Now we consider the dynamics in Group 1 based on the theoretical model [14,40]. As shown in Fig.s 10 and 11, f(A) in the control samples under various conditions is always below 5%. It indicates that, the increasing trend of f(A) with n_0 observed in Group 1 is unlikely

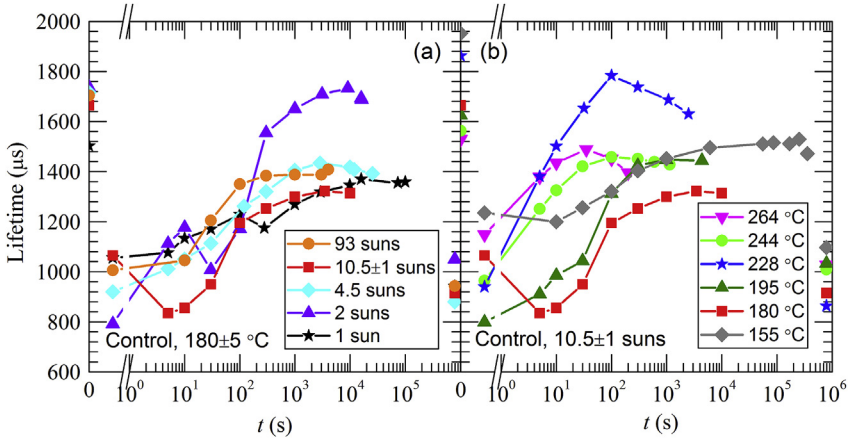

Fig. 9. (a) Evolution of lifetime of non-compensated n-type Cz wafers during annealing (a) at 180 ± 5 °C under 1–93 suns, and (b) under 10.5 ± 1 suns at 155–264 °C. The solid lines are guides to the eye. The lifetime data at 0 s were measured after dark annealing at 250 °C for 40 min. The data before the axis break were measured after light soaking. The data at about 10^6 s were measured after stability test.

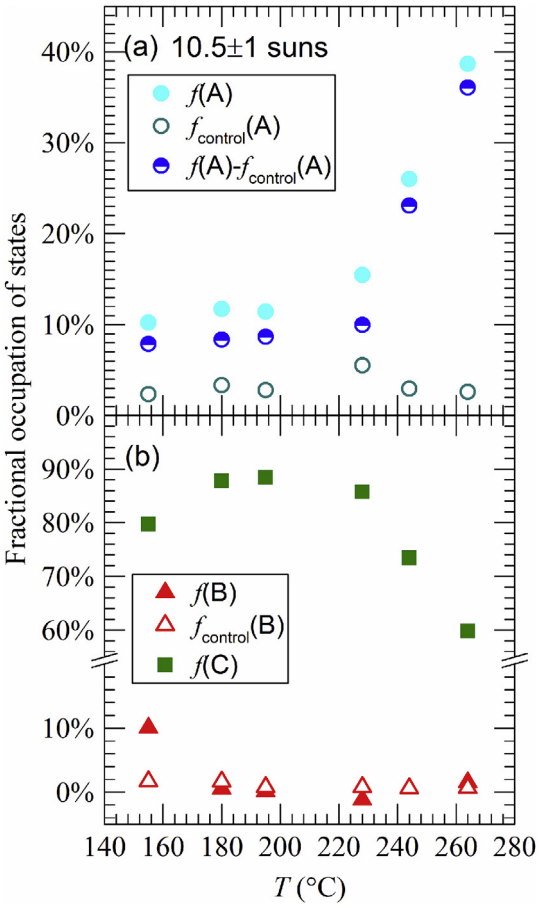

Fig. 11. The fractions occupied by the three states after regeneration, as a function of temperature.

dominated by the background lifetime effects. Fig. 12 shows the reaction rates of all 4 possible state transitions during regeneration [40]. They are explained as follows:

As shown in the figure, for all the samples, $k_{AB,FRC}$, $k_{AB,SRC} \gg k_{BA}$, and $k_{BC} \gg k_{CB}$. This means that the two backward reactions B→A and C→B could be neglected during the regeneration. As the estimated activation rates are quite similar in those samples, the most likely reason for the less complete transition to State C in higher-doped samples could be the lower regeneration rate k_{BC}.

In addition, we note an inconsistency between the experimental results and the theoretical model: the comparison between f(A) and f(B). In most samples, we have found f(A) > f(B). However, based on the theoretical model [40], for State A to achieve the final steady state, the following equation must be fulfilled

$$N_A^* k_{AB} = N_B^* k_{BA}. \quad (7)$$

This gives $N_B^* \gg N_A^*$ if $k_{AB} \gg k_{BA}$, as shown in Fig. 12. The most probable reason is the overestimation of the activation rates at 180 °C: 1) the activation energy for activating the BO defects was obtained at a lower temperature range (< 130 °C) [3,20]. It may be less accurate for applications at higher temperatures. 2) the effective lifetime during regeneration could be very different from that measured at room temperature [46,47], which results in uncertainties in the estimated injection levels. The possible overestimation of the activation kinetics of BO defects in compensated n-Si was also discussed in Ref. [24]. Unfortunately, a more accurate estimation of the activation rates at high temperatures cannot be given based on the current data in this study.

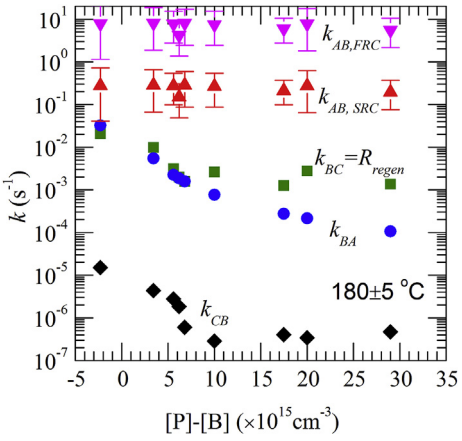

Fig. 12. $k_{AB,FRC}$, $k_{AB,SRC}$, k_{BA}, k_{BC}, and k_{CB} at 180 °C, as a function of [P]-[B].

1) A→B, with the rate $k_{AB,FRC}$ for the fast forming recombination center, and $k_{AB,SRC}$ for the slowly forming recombination center, calculated based on Ref. [20]. Note that we are only using this two recombination center model to calculate the activation rates. We note that there are other defect models [44,45] contradicting this model. However, the contradiction is mainly on the understanding of the defect instead of the activation kinetics data.
2) B→A, with the annihilation rate k_{BA}. The annihilation rates in a set of samples with similar doping levels as those in this study were measured at 200 °C in Ref. [4]. The rates were corrected to 180 °C using the activation energy 1.3 eV in Refs. [2,3].
3) B→C, with the regeneration rate k_{BC}. When the regeneration starts with State B, and is conducted at a temperature range where the forward reaction rate dominates the reaction, $k_{BC} = R_{regen}$ (the fitted reaction rate from the measured kinetics). This is valid for the samples in Group 1.
4) C→B, with the destabilization rate k_{CB}. We measured this rate in samples from Group 1 with the following procedure: 1) after regeneration and stability test, each sample was dark annealed at 180 °C for some time. 2) Then the sample was subjected to a stability test, after which the lifetime was measured and the destabilized defect concentration during the annealing could be determined. 3) Steps (1) and (2) were repeated to collect 5 points for each sample. 4) Then the kinetics were fitted with a single exponential relation [12] to extract the k_{CB}.

5. Conclusions

In conclusion, we have examined the effects of doping level, illumination intensity and temperature on the regeneration kinetics and dynamics of BO defects in compensated n-Si. The application of high illumination intensities at around 200 °C was identified as the optimal condition for rapid and complete regeneration.

Under the same regeneration condition, the regeneration rate R_{regen} remains almost constant in differently-doped n-type samples, after being corrected with [O_i] and average injection level. A linear dependence of R_{regen} on the average injection level during regeneration was concluded, in agreement with studies using p-Si.

A significant improvement in the regeneration completeness was achieved compared with previous studies [4,26,30], especially in the samples with $n_0 > 1 \times 10^{16}\,cm^{-3}$. 180–230 °C was identified as the optimal temperature range to maximize the regeneration completeness under 10 suns. At 180 °C, a quite similar completeness was achieved under 1–93 suns. For all regeneration conditions investigated in this work, the incompleteness is dominated by the occupation of the annealed state in almost all the samples. The occupation of the annealed state was found to increase with increasing temperature, and may decrease with increasing illumination intensity. The agreement and disagreement between the experimental findings and the theoretical model in Refs. [14,39] were discussed.

Acknowledgements

This work has been supported through the Australian Renewable Energy Agency (ARENA) project RND009, and the Australian Centre for Advanced Photovoltaics. Support from the Australian Research Council (ARC) DECRA program is also acknowledged. The authors would like to thank Tim Niewelt for fruitful discussions. The authors would like to thank B. Lim and J. Schmidt for supplying the Cz samples.

References

[1] S. Rein, S. Glunz, Electronic properties of the metastable defect in boron-doped Czochralski silicon: unambiguous determination by advanced lifetime spectroscopy, Appl. Phys. Lett. 82 (2003) 1054–1056.
[2] J. Schmidt, K. Bothe, Structure and transformation of the metastable boron-and oxygen-related defect center in crystalline silicon, Phys. Rev. B 69 (2004) 024107.
[3] K. Bothe, J. Schmidt, Electronically activated boron-oxygen-related recombination centers in crystalline silicon, J. Appl. Phys. 99 (2006) 013701.
[4] B. Lim, Boron–Oxygen-Related Recombination Centers in Crystalline Silicon and the Effects of Dopant-Compensation, PhD Thesis University of Hannover, 2012.
[5] V.V. Voronkov, R. Falster, Latent complexes of interstitial boron and oxygen dimers as a reason for degradation of silicon-based solar cells, J. Appl. Phys. 107 (2010) 053509.
[6] T. Niewelt, J. Schön, W. Warta, S.W. Glunz, M.C. Schubert, Degradation of crystalline silicon due to boron–oxygen defects, IEEE J. Photovoltaics 7 (2017) 383–398.
[7] G. Hahn, S. Wilking, A. Herguth, BO-related Defects: Overcoming Bulk Lifetime Degradation in Crystalline Si by Regeneration vol.242, Trans Tech Publ, 2016.
[8] B. Hallam, A. Herguth, P. Hamer, N. Nampalli, S. Wilking, M. Abbott, et al., Eliminating light-induced degradation in commercial p-type Czochralski silicon solar cells, Appl. Sci. 8 (10) (2017).
[9] A. Herguth, G. Schubert, M. Kaes, and G. Hahn, "A new approach to prevent the negative impact of the metastable defect in boron doped cz silicon solar cells," Presented at the Photovoltaic Energy Conversion, Conference Record of the 2006 IEEE 4th World Conference on, 2006.
[10] A. Herguth, G. Schubert, M. Käs, G. Hahn, Investigations on the long time behavior of the metastable boron–oxygen complex in crystalline silicon, Prog. Photovoltaics Res. Appl. 16 (2008) 135–140.
[11] B.J. Hallam, P.G. Hamer, S.R. Wenham, M.D. Abbott, A. Sugianto, A.M. Wenham, et al., Advanced bulk defect passivation for silicon solar cells, IEEE J. Photovoltaics 4 (2014) 88–95.
[12] S. Wilking, C. Beckh, S. Ebert, A. Herguth, G. Hahn, Influence of bound hydrogen states on BO-regeneration kinetics and consequences for high-speed regeneration processes, Sol. Energy Mater. Sol. Cell. 131 (2014) 2–8.
[13] B.J. Hallam, P.G. Hamer, S. Wang, L. Song, N. Nampalli, M.D. Abbott, et al., Advanced hydrogenation of dislocation clusters and boron-oxygen defects in silicon solar cells, Energy Procedia 77 (2015) 799–809.
[14] B.J. Hallam, M.D. Abbott, N. Nampalli, P.G. Hamer, S.R. Wenham, Implications of accelerated recombination-active defect complex formation for mitigating carrier-induced degradation in silicon, IEEE J. Photovoltaics 6 (2016) 92–99.
[15] T. Schutz-Kuchly, J. Veirman, S. Dubois, D. Heslinga, Light-Induced-Degradation effects in boron-phosphorus compensated n-type Czochralski silicon, Appl. Phys. Lett. 96 (2010) 3505.
[16] B. Lim, F. Rougieux, D. Macdonald, K. Bothe, J. Schmidt, Generation and annihilation of boron–oxygen-related recombination centers in compensated p-and n-type silicon, J. Appl. Phys. 108 (2010) 103722.
[17] V. Voronkov, R. Falster, K. Bothe, B. Lim, J. Schmidt, Lifetime-degrading boron-oxygen centres in p-type and n-type compensated silicon, J. Appl. Phys. 110 (2011) 063515.
[18] F. Rougieux, B. Lim, J. Schmidt, M. Forster, D. Macdonald, A. Cuevas, Influence of net doping, excess carrier density and annealing on the boron oxygen related defect density in compensated n-type silicon, J. Appl. Phys. 110 (2011) 063708.
[19] R. Einhaus, J. Kraiem, J. Degoulange, O. Nichiporuk, M. Forster, P. Papet, et al., 19% efficiency heterojunction solar cells on Cz wafers from non-blended upgraded metallurgical silicon, Photovoltaic Specialists Conference (PVSC), 2012 38th IEEE, 2012, pp. 003234–003237.
[20] J. Schön, T. Niewelt, J. Broisch, W. Warta, M. Schubert, Characterization and modelling of the boron-oxygen defect activation in compensated n-type silicon, J. Appl. Phys. 118 (2015) 245702.
[21] D. MacDonald, A. Liu, A. Cuevas, B. Lim, J. Schmidt, The impact of dopant compensation on the boron–oxygen defect in p-and n-type crystalline silicon, Phys. Status Solidi 208 (2011) 559–563.
[22] V.V. Voronkov, R.J. Falster, B. Lim, J. Schmidt, (Invited) boron-oxygen related lifetime degradation in p-type and n-type silicon, ECS Trans. 50 (2013) 123–136.
[23] C. Sun, H.T. Nguyen, H.C. Sio, F.E. Rougieux, D. Macdonald, Activation kinetics of the boron-oxygen defect in compensated n- and p-type silicon studied by high-injection micro-photoluminescence, IEEE J. Photovoltaics 7 (2017) 988–995.
[24] D. Shen, C. Sun, P. Zheng, D. Macdonald, F. Rougieux, Carrier induced degradation in compensated n-type silicon solar cells: impact of light-intensity, forward bias voltage, and temperature on the reaction kinetics, Jpn. J. Appl. Phys. 56 (2017) 08MB23.
[25] Y. Schiele, S. Wilking, F. Book, T. Wiedenmann, G. Hahn, Record efficiency of PhosTop solar cells from n-type Cz UMG silicon wafers, Energy Procedia 38 (2013) 459–466.
[26] P. Zheng, F. Rougieux, C. Samundsett, X. Yang, Y. Wan, J. Degoulange, et al., Upgraded metallurgical-grade silicon solar cells with efficiency above 20%, Appl. Phys. Lett. 108 (2016) 122103.
[27] P. Zheng, F.E. Rougieux, X. Zhang, J. Degoulange, R. Einhaus, P. Rivat, et al., 21.1% UMG silicon solar cells, IEEE J. Photovoltaics 7 (2017) 58–61.
[28] R. Basnet, W. Weigand, J.Y. Zhengshan, C. Sun, S.P. Phang, F.E. Rougieux, et al., Impact of tabula rasa and phosphorus diffusion gettering on 21% heterojunction solar cells based on n-type czochralski-grown upgrade metallurgical-grade silicon, 2018 IEEE 7th World Conference on Photovoltaic Energy Conversion (WCPEC)(A Joint Conference of 45th IEEE PVSC, 28th PVSEC & 34th EU PVSEC), 2018, pp. 1687–1691.
[29] M. Forster, P. Wagner, J. Degoulange, R. Einhaus, G. Galbiati, F.E. Rougieux, et al., Impact of compensation on the boron and oxygen-related degradation of upgraded metallurgical-grade silicon solar cells, Sol. Energy Mater. Sol. Cell. 120 (2014) 390–395.
[30] T. Niewelt, J. Broisch, J. Schön, J. Haunschild, S. Rein, W. Warta, et al., Light-induced degradation and regeneration in n-type silicon, Energy Procedia 77 (2015) 626–632.
[31] S. Wilking, M. Forster, A. Herguth, G. Hahn, From simulation to experiment: understanding BO-regeneration kinetics, Sol. Energy Mater. Sol. Cell. 142 (2015) 87–91.
[32] C. Sun, D. Chen, W. Weigand, R. Basnet, S.P. Phang, B. Hallam, et al., Complete regeneration of BO-related defects in n-type upgraded metallurgical-grade Czochralski-grown silicon heterojunction solar cells, Appl. Phys. Lett. 113 (2018) 152105.
[33] S. Wilking, A. Herguth, G. Hahn, Influence of hydrogen on the regeneration of boron-oxygen related defects in crystalline silicon, J. Appl. Phys. 113 (2013) 194503.
[34] H.C. Sio, Hydrogenation of High Performance Multicrystalline Silicon. (to be published).
[35] F. Schindler, M.C. Schubert, A. Kimmerle, J. Broisch, S. Rein, W. Kwapil, et al., Modeling majority carrier mobility in compensated crystalline silicon for solar cells, Sol. Energy Mater. Sol. Cell. 106 (2012) 31–36.
[36] A. Herguth, On the meaning (fullness) of the intensity unit 'suns' in light induced degradation experiments, Energy Procedia 124 (2017) 53–59.
[37] D. Sperber, A. Graf, D. Skorka, A. Herguth, G. Hahn, Degradation of surface passivation on crystalline silicon and its impact on light-induced degradation experiments, IEEE J. Photovoltaics 7 (2017) 1627–1634.
[38] S. Wilking, S. Ebert, C. Beckh, A. Herguth, G. Hahn, Of apples and oranges: why comparing BO regeneration rates requires injection level correction, 32nd European Photovoltaic Solar Energy Conference and Exhibition, 2016, pp. 487–494.
[39] V. Steckenreiter, D.C. Walter, J. Schmidt, Kinetics of the permanent deactivation of the boron-oxygen complex in crystalline silicon as a function of illumination intensity, AIP Adv. 7 (2017) 035305.
[40] A. Herguth, G. Hahn, Kinetics of the boron-oxygen related defect in theory and experiment, J. Appl. Phys. 108 (2010) 114509.
[41] A. Richter, S.W. Glunz, F. Werner, J. Schmidt, A. Cuevas, Improved quantitative description of Auger recombination in crystalline silicon, Phys. Rev. B 86 (2012) 165202.
[42] B. Hallam, M. Abbott, N. Nampalli, P. Hamer, S. Wenham, Influence of the formation-and passivation rate of boron-oxygen defects for mitigating carrier-induced degradation in silicon within a hydrogen-based model, J. Appl. Phys. 119 (2016) 065701.
[43] D. Chen, P.G. Hamer, M. Kim, T.H. Fung, G. Bourret-Sicotte, S. Liu, et al., Hydrogen induced degradation: a possible mechanism for light-and elevated temperature-induced degradation in n-type silicon, Sol. Energy Mater. Sol. Cell. 185 (2018) 174–182.
[44] B. Hallam, M. Abbott, T. Nærland, S. Wenham, Fast and slow lifetime degradation in boron-doped Czochralski silicon described by a single defect, Phys. Status Solidi Rapid Res. Lett. 10 (2016) 520–524.
[45] B. Hallam, M. Kim, M. Abbott, N. Nampalli, T. Nærland, B. Stefani, et al., Recent insights into boron-oxygen related degradation: evidence of a single defect, Sol. Energy Mater. Sol. Cell. 173 (2017) 25–32.
[46] V. Voronkov, R. Falster, Permanent deactivation of boron–oxygen recombination centres in silicon, Phys. Status Solidi 253 (2016) 1721–1728.
[47] P. Hamer, N. Nampalli, Z. Hameiri, M. Kim, D. Chen, N. Gorman, et al., Boron-oxygen defect formation rates and activity at elevated temperatures, Energy Procedia 92 (2016) 791–800.